Food Chemistry: X 26 (2025) 102334

Contents lists available at ScienceDirect

Food Chemistry: X

journal homepage: www.sciencedirect.com/journal/food-chemistry-x

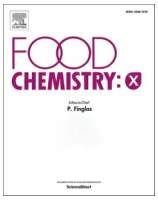

Molecular insights into the antifreeze mechanism of collagen peptides based on their interaction with ice crystals

Jiajian Liang [a,b], Xiujuan Chen [a,b], Mingtang Tan [a,b,c,*], Zhongqin Chen [a,b,c], Haisheng Lin [a,b,c], Jialong Gao [a,b,c], Huina Zheng [a,b,c], Wenhong Cao [a,b,c,*]

[a] Shenzhen Institute of Guangdong Ocean University, Shenzhen 518108, China
[b] College of Food Science and Technology, Guangdong Ocean University, Zhanjiang 524088, China
[c] Guangdong Provincial Key Laboratory of Aquatic Products Processing and Safety, Guangdong Provincial Engineering Technology Research Center of Seafood, Zhanjiang 524088, China

ARTICLE INFO

Keywords:
Cod collagen peptide
Channa argus surimi
Antifreeze activity
Protein denaturation
Molecular docking

ABSTRACT

This study explores the molecular-level cryoprotective effect of cod collagen peptide-1 (CCP-1) on surimi during freeze-thaw cycles, examining its interaction with ice crystals and its role in maintaining the structural integrity of surimi. Results indicated that CCP-1 exhibited the most effective cryoprotection on catalase, preserving 83.4 % of its residual enzyme activity, and prevented myofibrillar protein (MP) from freeze denaturation by sustaining the activity of Ca^{2+}-ATPase and maintaining structural integrity. The antifreeze effect of CCP-1 (1.0 % and 3.0 %, *w*/w) is comparable to that of commercial antifreeze containing 0.5 % compound phosphate (*w*/w). Moreover, CCP-1's ability to interact with ice crystals is closely tied to its primary structure, where hydrophilic and hydrophobic amino acids work in tandem. Specifically, alkaline and acidic amino acids are capable of forming stronger hydrogen bonds, thereby enhancing their interaction with ice crystals. This work offers a theoretical basis for analyzing the binding behavior of antifreeze peptides with varying amino acid compositions.

1. Introduction

Freezing is the primary method for processing, storing, and transporting aquatic products. However, during freezing, the growth and recrystallization of ice crystals may cause protein deterioration through freeze denaturation (Li et al., 2025). Inhibiting ice crystal growth is vital to maintaining the quality of frozen aquatic products. Currently, adding antifreeze is regarded as an effective way to prevent protein freeze denaturation. Various phosphates are widely used in aquatic products because of their excellent antifreeze properties, among which compound phosphates prepared mainly by mixing sodium tripolyphosphate and sodium hexametaphosphate are often used as commercial antifreeze agents (Liu et al., 2023). Nevertheless, excessive intake of phosphate can affect the body's absorption of calcium leading to an imbalance in the body's calcium-phosphorus ratio, which carries the risk of osteoporosis and aggravation of cardiovascular and kidney diseases. Antifreeze peptides (AFP), which are proteins that can be hydrolyzed to exhibit antifreeze activity, have been shown to effectively inhibit the growth of ice crystals and regulate their morphology (Chen et al., 2020). These peptides present a promising avenue for the development of new green, efficient, and safe phosphorus-free antifreeze solutions, particularly in the food industry where controlling ice crystal growth is crucial for maintaining product quality. Notably, food-origin protein serves as the primary raw material for AFP. It has the advantages of abundant raw materials, wide sources, and highly active peptide fragments obtained through enzyme digestion technology (Yang et al., 2021). Furthermore, owing to the constraints of cold chain technology, frequent freezing and thawing cycles often arise throughout the freezing and distribution procedures (Shi et al., 2024). Yang et al. (2023) showed that incorporating *Takifugu obscurus* skin AFP during freeze-thaw (F-T) cycling was able to inhibit the denaturation and structural changes of myofibrillar proteins (MP) in surimi. Chen, Wu, et al. (2022) found that collagen AFPs were able to maintain surface hydrophobicity and sustain proteolysis of surimi proteins during F-T cycling and improve the stability of surimi gels. Hence, simulating the F-T cycling process to investigate the functional effects of AFPs on fish muscle structure is a common approach to evaluate the potential of AFPs for application as antifreeze agents.

AFPs not only inhibit MP freeze denaturation but also ice crystal

* Corresponding authors at: College of Food Science and Technology, Guangdong Ocean University, No.1 Haida Road, Zhanjiang 524088, China.
E-mail addresses: mttan@gdou.edu.cn (M. Tan), cwenhong@gdou.edu.cn (W. Cao).

https://doi.org/10.1016/j.fochx.2025.102334
Received 6 January 2025; Received in revised form 17 February 2025; Accepted 25 February 2025
Available online 3 March 2025

growth. Currently, many studies have reported that collagen AFPs exhibit antifreeze activity. For instance, Chen, Li, et al. (2022) discovered that AFPs derived from the hydrolysis of carp (*Cyprinus carpio*) scales could notably enhance the water retention of surimi by controlling the dimensions of ice crystals. Fu et al. (2019) reported that AFPs derived from the hydrolysates of *Scomberomorus niphonius* skin contained high levels of glycine, alanine, and proline, effectively inhibiting ice crystal formation. To date, the exact mechanism of interaction between AFPs and ice crystals remains unclear, posing significant challenges in elucidating AFPs' mode of action. However, molecular docking offers a means to characterize the binding sites of peptides and receptors, potentially serving as a valuable tool for exploring the interaction between AFPs and ice crystals. (Vidal et al., 2022; Yang et al., 2022). The molecular docking technique was employed to analyze the interaction between AFP and ice crystals, identifying the specific binding site, the optimal binding conformation, and the primary amino acids that form hydrogen bonds during the binding proces (Jiang et al., 2022). It helps to make up for the limitations of the experiment and makes it possible to explore the binding law of AFP and ice crystal.

Marine collagen was deemed a safe AFP alternative, considering infectious disease risks associated with processing by-products like cowhide and pigskin, as well as religious constraints (Coppola et al., 2020). The pollock (*Theragra chalcogramma*) is the main processing raw material for frozen cod fillets exported from China. During processing, only 30–50 % (wet weight) of the fish was utilized for fillet production, leading to substantial by-product generation (Stevens et al., 2018). Pollock skin is notable for its abundant collagen content and efficient collagen recovery during enzyme digestion (Zarubin et al., 2024). Our previous research demonstrated that the thermal hysteresis activity (THA) of cod skin collagen peptides was 1.90 °C, and this activity was enhanced to 2.60 °C for the purified cod collagen peptide-1 (CCP-1) fraction, as detailed in our study on the anti-freeze properties of these peptides. Crucially, a strong correlation was observed between the amino acid composition pairs of AFPs and THA (Liang et al., 2025). This indicated that collagen peptides derived from cod could suppress the growth of ice crystals. However, the practical antifreeze efficacy of CCP-1 in frozen foods, as well as the specific roles of various amino acids in the interaction between AFPs and ice crystals, still await further exploration.

This study focused on examining the cryoprotective properties of CCP-1, derived from cod collagen peptide through ion exchange, on *Channa argus* surimi. We determined the extent of freeze denaturation in the MP of surimi following CCP-1 treatment. Furthermore, we employed molecular docking technology to dock numerous AFPs derived from CCP-1 with ice crystals, aiming to elucidate the binding mechanism between cod collagen peptides and ice crystals during the freezing process. This study aimed to provide a scientific basis for the mechanism of AFP controlling the growth of ice crystals.

2. Material and methods

2.1. Materials

Fresh snakehead (*Channa argus*) was purchased from Lakewood Town Market (Zhangjiang, China). The Ca^{2+}-ATPase test kit was purchased from Jiancheng Bioengineering Institute (Nanjing, China). The total sulfhydryl kit was purchased from Griseo Bio-technology Co., Ltd. (Suzhou, China). All other chemicals were analytical grade. Hydrogen peroxidase was purchased from Solarbio Science & Technology Co., Ltd. (Beijing, China). The fraction of cod collagen peptide-1 (CCP-1) was isolated from cod collagen peptides by ion exchange (Liang et al., 2025).

2.2. Cryoprotection of catalase by CCP-1

The method referenced is from Cao, Cai, et al. (2023). The catalase solution was diluted 5-fold with a pH 7.0, 0.05 M KH_2PO_4-NaOH buffer. The enzyme dilution was then mixed with a 2 mg/mL peptide solution in equal volumes and homogenized. The initial enzyme activity of catalase was determined separately. Subsequently, the solution was placed in a − 20 °C refrigerator to freeze for 24 h, then removed and thawed under running water at 25 °C for 0.5 h. This F-T was repeated three times, with the catalase activity being measured after each cycle. The antifreeze activity was expressed as the residual enzyme activity of catalase relative to the unfrozen control. The reaction system consisted of 1.9 mL of distilled water, 0.1 mL of the peptide and enzyme mixture, and 1 mL of 0.1 M H_2O_2. The catalase activity was measured using a UV spectrophotometer (Cary 60, Agilent Inc., USA) at 240 nm. The initial absorbance value was recorded at 1-min intervals for 5 min, and the residual catalase activity was calculated by substituting the absorbance values into the following formula.

$$Catalase\ activity = \Delta A_{240} \times \frac{Dilution\ ratio \times Total\ Volume}{t \times Sample\ volume} \times 10 \quad (1)$$

$$Catalase\ residual\ activity\ (\%) = \frac{Enzyme\ activity\ after\ F-T}{Enzyme\ activity\ before\ F-T} \times 100 \quad (2)$$

2.3. Preparation of surimi

In the process of making surimi, the dorsal muscle of Snakehead fish was taken and minced into surimi using a meat grinder. Subsequently, the surimi underwent three rinses with ultrapure water, followed by centrifugation at 4 °C and 9000 rpm for 15 min to obtain the precipitate. The sample groups were supplemented with 0.5 %, 1 %, and 3 % (*w*/w) of CCP-1 by mass of surimi. A positive control group (PC) with 0.5 % (*w*/w) of compound phosphate was added, while the negative control group (NC) did not receive any treatment. The samples were mixed homogeneously and then subjected to F-T cycles at −20 °C for 5 cycles of 72 h each. The samples were thawed in running water at 25 °C for 1 h after each F-T cycle.

2.4. Extraction of MP

The method described by Chen, Li, et al. (2022) was slightly modified. Initially, 1 g of surimi was homogenized through the addition of 10 mL of 0.02 mol/L Tris-HCl buffer (containing 0.05 mol/L KCl, pH = 7) for one minute per cycle. This was followed by centrifugation for 10 min at 9000 rpm and 4 °C, after which the supernatant was poured out. The aforementioned steps were then repeated twice. Subsequently, 10 mL of a 0.02 mol/L Tris-HCl solution, which included 0.5 mol/L KCl and was adjusted to a pH of 7, was introduced to the mixture. The mixture was incubated in the refrigerator at 4 °C for 1 h. After that, it was centrifuged for 15 min at 9000 rpm and 4 °C, and the supernatant was collected after centrifugation.

2.5. Determination of MP concentration

The protein concentration was determined using the method of the double urea reagent (Hu et al., 2022). The protein concentration was then calculated using a standard curve, which was plotted as $y = 0.0142x + 0.1071, R^2 = 0.9996$.

2.6. Determination of total sulfhydryl content (TSC) of MP

The total sulfhydryl content of MP was determined using the method described by Zhu et al. (2022). Absorbance was measured at 412 nm using a multiscan spectrum (Varioskan lux, Thermo Fisher Scientific, USA). The standard curve was simplified by substituting the values into the formula to obtain the following equation. The total sulfhydryl content was then calculated by substituting the absorbance into this equation. In the equation, A_{assay} represents the absorbance of the assay group sample, and $A_{control}$ represents the absorbance of the control group

sample.

$$\text{TSC}\ (\mu\text{mol/mL}) = 1.0445\ (A_{assay} - A_{control}) - 0.0004 \quad (3)$$

2.7. Determination of Ca^{2+}-ATPase activity of MP

Used Ca^{2+}-ATPase assay kit, absorbance was measured at 636 nm and calculated by substituting the following equation. In the equation, $C_{standard}$ is the concentration of standard, 0.02 μmol/mL, and C_{pr} is the concentration.

$$Ca^{2+} - \text{ATPase activity of MP}(\text{U/mgprot}) = \frac{A_{assay} - A_{control}}{A_{standard} - A_{blank}} \times C_{standard} \times 6 \times 2.8 \div C_{pr} \quad (4)$$

2.8. Change in secondary structure of MP

The UV absorption of a 0.5 mg/mL MP solution was determined using a UV spectrophotometer (Cary 60, Agilent Inc., USA) in the wavelength range of 220–400 nm. A 0.2 mg/mL MP solution was placed in a quartz cuvette with a 0.5 mm optical path length, and its secondary structure was determined using a circular dichroism spectrometer (Chirascan V100, Applied Photophysics Inc., UK) in the range of 190–260 nm (Li et al., 2018; Wang et al., 2024).

2.9. Determination of intrinsic fluorescence spectra

The fluorescence intensity of MP was quantified using a fluorescence spectrophotometer (RF-5301PC, Shimadzu Co., Japan), adhering to the established protocol by Yang et al. (2023). The MP concentration was standardized to 1.0 mg/mL, with an excitation wavelength set at 295 nm, and the emission spectrum was recorded between 300 and 400 nm.

2.10. Microstructure

The frozen samples were sectioned into long, wide, and thick strips with dimensions of 1.5 × 1.0 × 1.0 cm, and then fixed in a 4 % paraformaldehyde solution. Following gradient dehydration with ethanol, the specimens were embedded in paraffin wax, sliced, stained with hematoxylin-eosin, dewaxed, dehydrated, sealed, and observed under a Nikon optical microscope at 10× magnification (Ouyang et al., 2024).

2.11. Establishment of AFP candidate library in CCP-1

2.11.1. LC-MS/MS analyze

The liquid chromatography parameters used in this study were similar to those described by Liang et al. (2025), which involved a Thermo Scientific EASY column C18 with dimensions of 3 μm i.d. × 75 μm. The mobile phases consisted of 0.1 % formic acid (A) and a mixture of 0.1 % formic acid with 84 % acetonitrile in water (B). The flow rate was maintained at 250 nL/min, and a linear gradient of mobile phase B was applied from 0 to 110 min. Was applied, increasing from 0 % to 35 %; from 110 to 118 min, the gradient further increased from 35 % to 100 %; and from 118 to 120 min, mobile phase B was held constant at 100 %.

The separated samples were analyzed by mass spectrometry on a mass spectrometer (Q-Exactive, Thermo Fisher Scientific, USA) for 120 min. The parameters were set to a resolution of 70,000 with an automatic gain control (AGC) target of 3e6 and a maximum injection time (Max IT) of 10 ms. The scanning range was set between 300 and 1800 *m/z*. For the secondary mass spectrum, a resolution of 17,500 was utilized, with a normalized collision energy of 30 eV, and an underfill ratio of 0.1 % was maintained.

2.11.2. Polypeptide sequence analysis

The mass spectrometry test raw files were searched in the Uniprot (https://www.uniprot.org/) database with Maxquant software (version 1.5.5.1) to obtain the peptide sequences. A 20-ppm of peptide mass tolerance was used for all searches and a 1 % false discovery rate (FDR) filtering was applied to match the peptide.

2.11.3. Screening AFP from CCP-1

To screen the peptides belonging to the AFP family from the peptide sequences identified by LC-MS/MS, the toxicity of the peptides was first predicted using ToxinPred (https://webs.iiitd.edu.in/raghava/toxinpred/multi_submit.php). Then the instability index and the grand average of hydropathicity (GRAVY) of the peptides were analyzed by Expasy (https://www.expasy.org/). Peptides belonging to the AFP family were then screened using the Cryoprotect web server (http://codes.bio/cryoprotect/) and the AFPs obtained by screening according to the previous steps were ranked according to the ion scores in mass spectrometry identification.

2.12. The AFPs in CCP-1 dock with the ice crystals

2.12.1. AFP secondary structure and ice crystal modeling

The peptides obtained from the previous screening were predicted using simulation with Alphafold 2.0 (http://colab.research.google.com/github/sokrypton/ColabFold/blob/main/AlphaFold2.ipynb), and secondary structures were constructed. The PDB format of the ice crystal structure model from GenIce 1.0.10 (https://pypi.org/project/GenIce/1.0.10/) was utilized as the docked macromolecular receptor for the study.

2.12.2. Molecular docking

Docking of AFPs and ice crystals was performed using Autodock vina 1.5.6 software with reference to the method of Zhu et al. (2024). The docking results were then analyzed for ice crystal-peptide interactions using Discovery Studio 2019 software.

2.13. Statistical analysis

The statistical analysis was carried out with SPSS software (version 27.0.1; SPSS Inc., Chicago, IL, USA). All data are expressed as the mean ± standard deviation (SD). Origin 2022 (Origin Lab Inc., Northampton, MA, USA) was utilized for designing other graphs. The Graphical Abstract and Fig. 6 were created using Figdraw 2.0 (Dotex Technology Co., Ltd., Hangzhou, China).

3. Results and discussion

3.1. Cryoprotective effect of CCP-1 on catalase in the F-T cycles

Antifreeze protein hydrolysates (antifreeze peptides) showed a cryoprotective effect on enzymes, therefore, their antifreeze activity can be assessed by measuring the enzyme activity before and after undergoing the F-T cycle (Cao, Cai, et al., 2023). Specifically, cod collagen peptide-1 (CCP-1) and cod collagen peptide-2 (CCP-2) represent two distinct fractions of cod collagen peptide (CCP), separated through ion exchange chromatography. As shown in Fig. 1(a), after three F-T cycles, the residual enzyme activity of catalase in the CCP-1 treatment group (83.4 %) was significantly higher than that in the CCP group (74.7 %, $P < 0.05$) and the CCP-2 treatment group (73.7 %, $P < 0.05$). Cao, Cai, et al., 2023 reported that collagen hydrolysates of squid skin could protect the enzyme from the effects of low temperatures and that determining the catalase activity before and after F-T cycles could reflect its antifreeze activity. This indicated that the CCP-1 fraction had the best protection of catalase during F-T cycles and its antifreeze activity was the highest. Therefore, the CCP-1 fraction was selected for the antifreeze experiment to further evaluate its antifreeze activity as well as to analyze its mechanism of action.

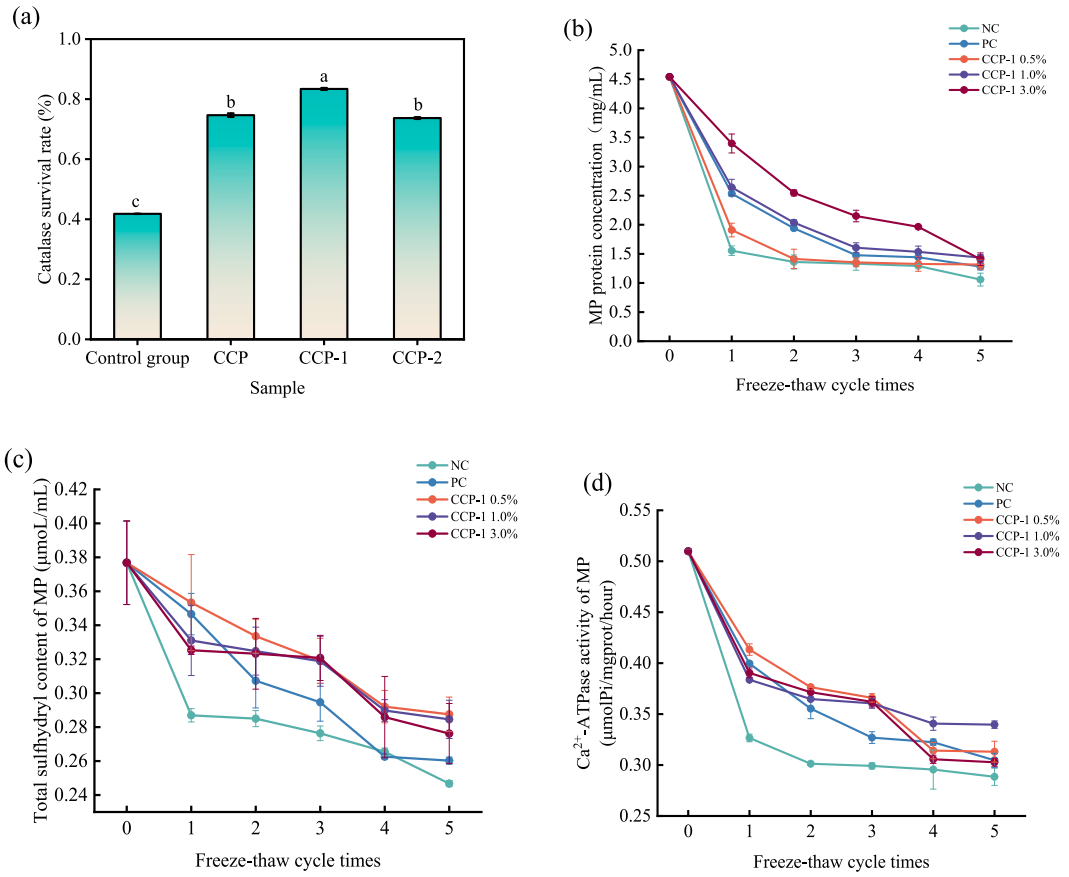

Fig. 1. Catalase residual enzyme activity of cod collagen peptide (CCP), CCP-1 and CCP-2 treatment groups after three freeze-thaw cycles (a). Change in MP concentration(b), total sulfhydryl content (c) and Ca^{2+}-ATPase activity(d) of MP after five freeze-thaw cycles of CCP-1.

3.2. *Cryoprotective effect of CCP-1 on MP during F-T cycles*

The decrease in solubility and total sulfhydryl content (TSC) of MP were key indicators of protein freeze denaturation (Cao, Majura, et al., 2023). The changes in MP concentration in different treatment groups are shown in Fig. 1(b). With the increased F-T cycles, the MP concentration in the NC, PC, and CCP-1 treatment groups decreased, indicating that MP underwent freezing denaturation during freezing. After 5 cycles of F-T, the MP concentration in the NC group decreased the most (76.71 %), while the MP concentration in the PC group decreased by 71.82 %. However, the MP concentration in the CCP-1 0.5 %, 1.0 %, and 3.0 % (*w*/w) treatment groups decreased by 71.01 %, 68.37 %, and 68.99 %, respectively. The antifreeze effect of the CCP-1 treatment group was found to be comparable to that of a commercial compound phosphate antifreeze agent, with a positive correlation observed between the CCP-1 treatment group's antifreeze efficacy and its concentration, as reported in studies optimizing the use of composite phosphate antifreeze agents in fish preservation. This was in line with the results of Cao, Majura, et al. (2023), which showed that tilapia skin collagen hydrolysate could inhibit the freeze denaturation of salt-soluble proteins, and its cryoprotective effect was positively correlated with its concentration.

As illustrated in Fig. 1(c), the tensile strength characteristic (TSC) of the material (MP) diminishes as the frequency of freeze-thaw (F-T) cycles increases. During the freezing process, the expansion of ice crystals modifies the conformation of MP, thereby exposing thiol groups which are susceptible to oxidation into disulfide bonds, subsequently decreasing the TSC of MP (Cao, Majura, et al., 2023). In addition, the formation of disulfide bonds contributed to protein aggregation and a decrease in the concentration of MP. However, in the CCP-1-treated group, the total sulfhydryl content of MP decreased more slowly, and after 5 F-T cycles, it was still higher than that in the NC and PC groups. This might be due to the fact that the hydrophilic amino acids in CCP-1, especially the alkaline amino acids (lysine, arginine, and histidine), bound to water molecules and hindered the movement of water molecules to the ice crystals (Liang et al., 2025). CCP-1 inhibited the freeze denaturation of MP by inhibiting the growth of ice crystals, which in turn inhibited the oxidation of the thiol groups and the formation of disulfide bonds. As the concentration of CCP-1 increases, the amount of hydrophilic amino acids also increases, potentially enhancing its antifreeze effectiveness.

3.3. *The cryoprotective effect of CCP-1 on Ca^{2+}-ATPase activity of MP*

Ca^{2+}-ATPase activity as a sensitive indicator capable of reflecting the structural integrity of myofibrils during frozen storage (Li et al., 2022; Yang et al., 2023). The Ca^{2+}-ATPase activity of MP decreased with the increase in the number of F-T cycles, and the decrease was greatest in the absence of antifreeze. After five F-T cycles, the Ca^{2+}-ATPase activity of MP decreased relatively slowly in the surimi treated with phosphate complex and different concentrations of CCP-1, while that of the NC group decreased by 43.42 %. This might be due to the fact that the hydrophilic amino acids of the AFPs in CCP-1 tended to bind to water molecules, thereby inhibiting the growth of ice crystals and the freeze denaturation of MP. Karnjanapratum and Benjakul (2015) reported that hydrophilic amino acids in peptides from fish skin gelatin hydrolysate were able to bind to water molecules around MP to maintain the stability of the myofibrillar structure, thereby protecting the active site of Ca^{2+}-ATPase. Therefore, CCP-1 inhibited MP's freeze denaturation and hindered large ice crystal formation by binding water and stabilizing the environment during freezing, aiding in the preservation of Ca^{2+}-ATPase

activity.

3.4. Change in the secondary structure of MP

Circular Dichroism (CD) was a common method for determining changes in the secondary structure of proteins (Zhang et al., 2020). Fig. 2(a, b, and c) shows the changes in secondary structure composition (α-helix, β-sheet, β-turn, random coil) of MP during F-T cycling. After 3 to 5 freeze-thaw cycles, the proportion of α-helix structure and β-sheet structure in the NC group decreased the most compared to the fresh sample, and the β-turn content increased. This was due to the disruption of hydrogen bonds formed by the peptide chains within the MP were disrupted and the electrostatic interaction between the amino acids was weakened during F-T cycling (Li et al., 2023). The MP structure unfolded, the hydrophobic groups were exposed, and the hydrophobic interaction led to aggregation and denaturation of the MP. However, the MP secondary structure in the PC and CCP-1 treated groups changed less during the F-T cycle. Notably, the α-helical structure of the CCP-1-treated group was significantly higher than that of the PC group during the F-T cycle ($P < 0.05$). This may be attributed to the incorporation of CCP-1, which helps maintain the integrity of the hydrogen bond between the hydroxyl oxygen and amino hydrogen on the polypeptide chain of MP, thus keeping the MP in a stable state (Li et al., 2023). The restoration of defolded MP, the depolymerisation of aggregated MP and the maintenance of MP stability prevented it from undergoing freezing degeneration. This consistency with the results aligns with the findings from the scientific research data analysis report. of the change in total sulfhydryl content, which suggested that CCP-1 was able to inhibit MP from undergoing freeze denaturation by maintaining protein structural stability. Upon the initiation of methionine oxidation, the α-helix undergoes a transition into a β-sheet structure, which subsequently evolves into a disordered β-turn configuration as oxidation progresses (Mi et al., 2024). However, the PC group had the highest proportion of β-turn structures ($P < 0.05$), indicating that the MP of the PC-treated group had been oxidized. Therefore, CCP-1 could inhibit MP oxidation and maintain its secondary structure stability during the F-T cycle, and the effect was positively correlated with the concentration.

3.5. Fluorescence spectrum

The fluorescence spectrum could indicate tertiary structural alterations in proteins, relying on shifts in polarity within the microenvironment exposing tryptophan residues (Pinilla et al., 2022; Tan et al., 2024). As shown in Fig. 2(d, e, and f), following three F-T cycles, a slight blue shift was observed in the λ_{max} values across all treatment groups, indicating that the F-T cycling process was able to shift tryptophan residues from a polar environment ($\lambda_{max} > 330$ nm) to a nonpolar-environment ($\lambda_{max} < 330$ nm).

This was the same result as Li et al. (2019), who found that the F-T cycling effect changes the environment in which the tryptophan residues are found. After 5 F-T cycles, the partially buried tryptophan residues of MP in the NC group without antifreeze were exposed to the polar environment, and λ_{max} was redshifted (Pan et al., 2021). However, a slight blue shift occurred in the PC and CCP-1 1.0 %, 3.0 % (*w*/w) treatment groups, indicating that the environment of tryptophan became more hydrophobic because MP refolded and a small amount of previously exposed tryptophan residues returned to the interior of MP (Zhang et al., 2017). In the CCP-1 3.0 % (*w*/w) treatment group, a blue shift occurred in λ_{max} and FI_{max} decreased the most slowly during the F-T cycle. This indicated that the hydrophilic amino acids in CCP-1 could bind to water and prevent drastic changes in the microenvironment of tryptophan during the F-T cycle. It could restore partially folded or cross-linked proteins, thus maintaining the stability of the MP tertiary structure and inhibiting the oxidation of tryptophan. The obtained results align with the TSC and Ca^{2+}-ATPase activity indicators, demonstrating that CCP-1 can safeguard MP against freeze denaturation by preserving its structural integrity. Meanwhile, as shown in Fig. 2(g), the alteration of the aromatic amino acid residues of MP results in a characteristic absorption peak at 275 nm (Wang et al., 2024), and CCP-1 3.0 % (*w*/w) had the largest peak absorption value, which suggested that the degree of oxidation of MP was relatively low. In summary, CCP-1 had a protective effect on the tertiary structure of MP.

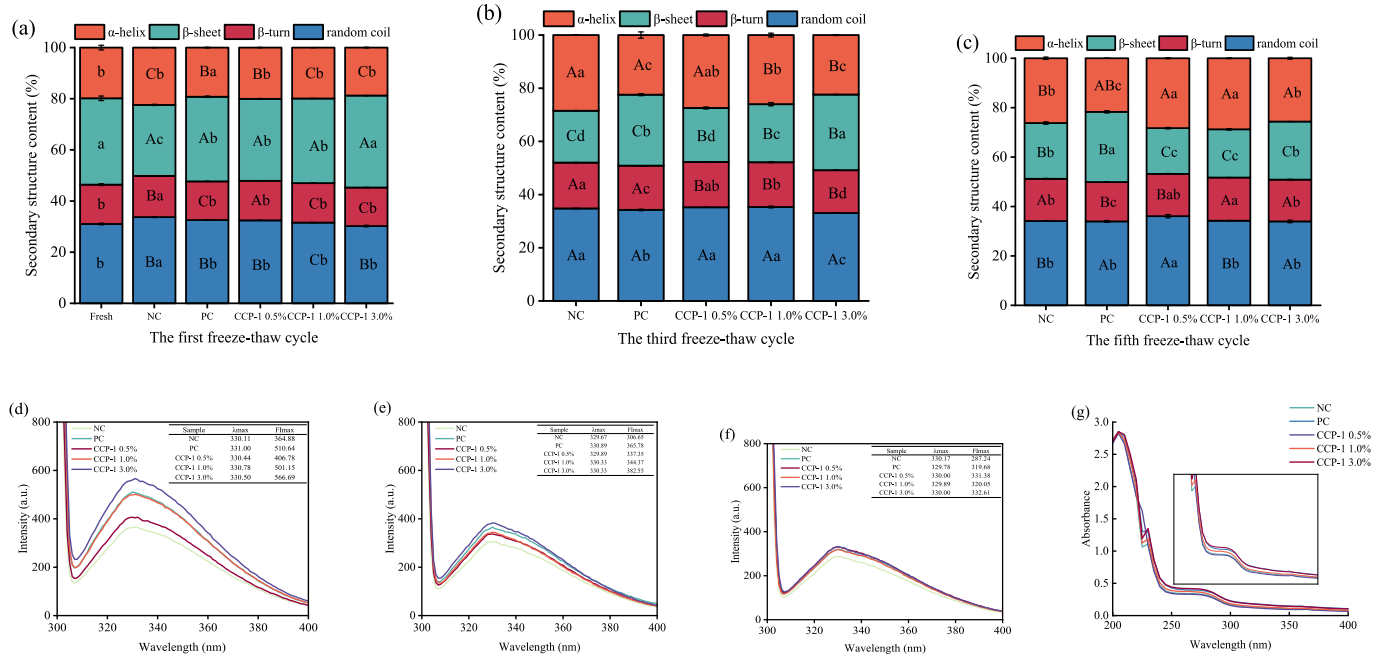

Fig. 2. Secondary structure (a, b, c) and tertiary structural (d, e, f) changes of MP after 1, 3, and 5 freeze-thaw cycles ($P < 0.05$); Lowercase letters indicate differences between treatment groups with the same number of freeze-thaw cycles, and uppercase letters indicate differences between different numbers of freeze-thaw cycles in the same treatment group. The UV absorption spectrum of the 5th round MP in the freeze-thaw cycle at 275 nm(g).

3.6. Microstructure

Microstructural changes could visualize the cryoprotective effect of CCP-1 on *Channa argus* fillets. The microstructure of *Channa argus* fillets is shown in Fig. 3. The muscle fibers of the fresh group were neatly aligned with no obvious gaps. However, the cross-section of myogenic fibers after 5 F-T cycles was no longer full and showed voids. The arrows in Fig. 3 indicated the formation of hollows and gaps in the cross-section of myofibrils due to mechanical damage caused by the growth of ice crystals. The myofibrillar gaps in the NC group were significantly larger, and the number of hollows in the cross-section of myofibrils increased with the increase in the number of F-T cycles. However, in the PC group, the myofibrils maintained a compact structure after 5 F-T cycles, although the myofibril cross-section showed voids. The gaps in the muscle fiber bundles treated with CCP-1 were small, and the muscle fiber cross-sections were relatively intact. Furthermore, the gap size and cross-sectional integrity of muscle fibers were proportional to the concentration of CCP-1, which was consistent with the results of Cao, Majura, et al. (2023). Meanwhile, the CCP-1 3.0 % (*w*/w) group showed similar results to the PC group, with no obvious gaps and a more intact muscle fiber cross-section compared to the NC group. This suggested that CCP-1 had a cryoprotective effect on *Channa argus* fillets.

3.7. Screening of cod collagen AFP

The LC-MS/MS analysis identified 2541 peptides within CCP-1, with 1966 peptides confirmed as AFPs, as reported by the cryoprotect website (Fig. S2, Supplementary material). And as shown in Table 1, the lengths of the screened AFPs were all in the range of 7–14, which is the ideal length for AFPs (Cao, Majura, et al., 2023). In addition, a higher peptide ion score in mass spectrometry analysis reflects the reliability and accuracy of peptide identification. The non-toxic peptides were obtained through multi-site prediction. The GRAVY value was less than 0, which indicates that hydrophilic AFPs were obtained from the screening, as GRAVY reflects the hydrophilicity of AFP and its ability to form hydrogen bonds with water (Cheung et al., 2009). Furthermore,

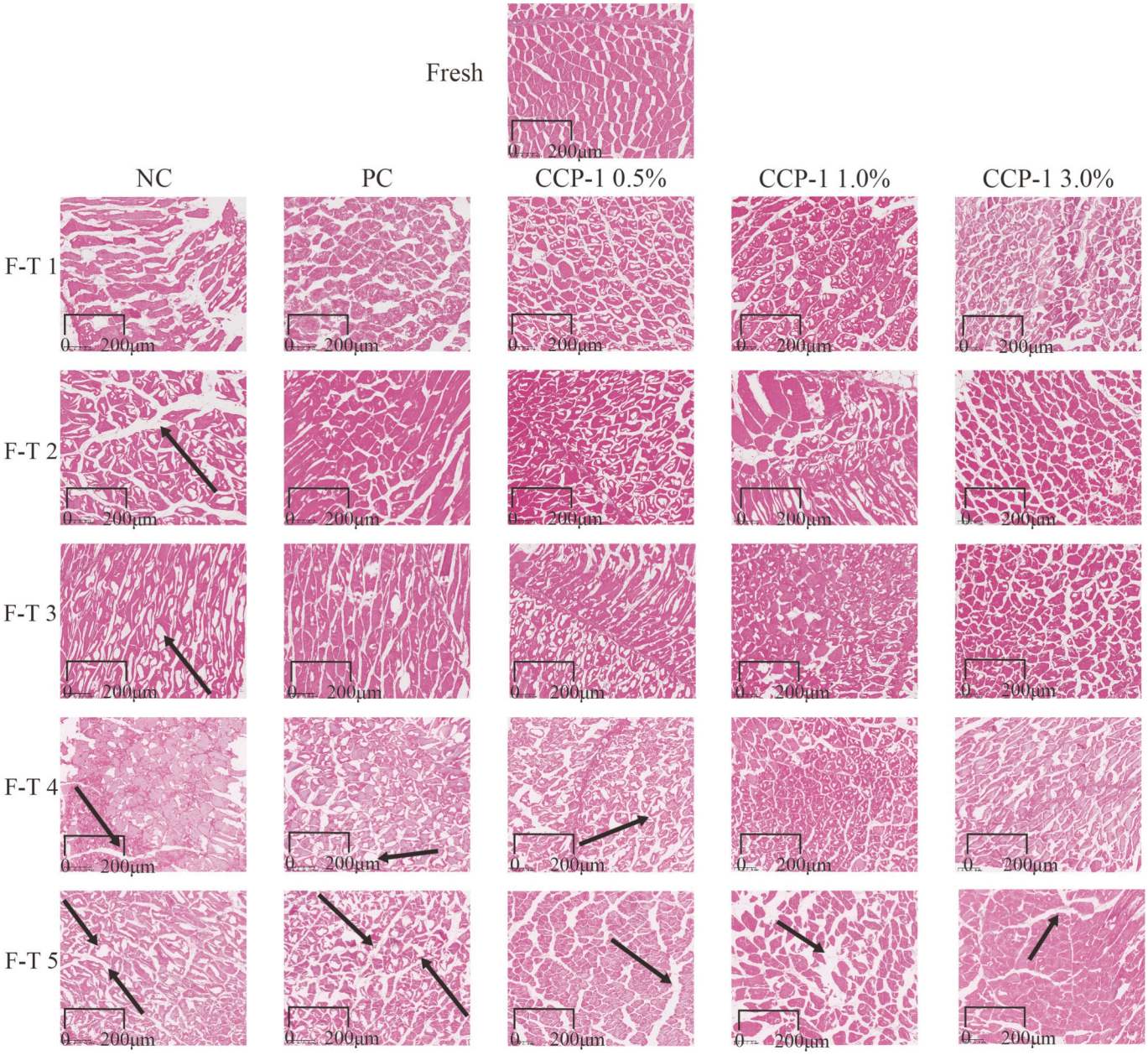

Fig. 3. Microstructural changes of fish fillets after 5 freeze-thaw cycles. Magnification of 10×.

Table 1
Results of the AFP screening for CCP-1.

Number	Sequence	Score	Mass	Length	Instability index	GRAVY	Toxic peptide	Isoelectric point
1	DGAPGKDGIR	137.690	984.499	10	2.79	−1.190	non-toxic peptides	5.96
2	TGPIGPPGPA	126.200	862.455	10	39.03	−0.200	non-toxic peptides	5.19
3	PTCTGPGA	121.870	702.301	8	28.27	−0.138	non-toxic peptides	5.91
4	ERERLEAQ	89.752	1029.520	8	8.75	−2.175	non-toxic peptides	4.79
5	KVFPNRTQ	78.616	988.545	8	12.79	−1.337	non-toxic peptides	11.00
6	QARDMGAP	75.311	844.386	8	22.21	−1.000	non-toxic peptides	5.84
7	NLRKLGLS	69.176	899.555	8	22.21	−0.212	non-toxic peptides	11.00
8	PGLNLNPQ	65.263	851.450	8	29.23	−0.812	non-toxic peptides	5.96
9	GDQVRGPA	64.776	798.398	8	12.79	−0.988	non-toxic peptides	5.84
10	GFAGPPGS	63.642	688.318	8	32.83	−0.075	non-toxic peptides	5.52
11	QDATKVSV	62.464	846.445	8	22.21	−0.275	non-toxic peptides	5.84
12	EHGKKGSP	60.358	838.430	8	20.06	−2.212	non-toxic peptides	8.69
13	TSILAKGR	57.811	844.513	8	22.21	−0.025	non-toxic peptides	11.00
14	ASGGRPGI	55.441	713.382	8	37.64	−0.225	non-toxic peptides	9.79
15	VGAARDAP	54.787	755.393	8	11.60	−0.050	non-toxic peptides	5.81
16	VAWQDREG	54.525	959.446	8	23.40	−1.288	non-toxic peptides	4.37
17	SVGQGPLP	54.525	753.402	8	22.21	−0.037	non-toxic peptides	5.24
18	PGSEHAAT	53.710	768.340	8	23.40	−0.825	non-toxic peptides	5.25
19	QAGGPRLA	52.683	768.424	8	14.75	−0.375	non-toxic peptides	9.75
20	GFKEPKSL	52.683	904.502	8	14.04	−0.938	non-toxic peptides	8.59
21	TSQGNAIN	51.787	803.377	8	22.21	−0.762	non-toxic peptides	5.19
22	SAGLPKGY	51.572	791.418	8	11.60	−0.350	non-toxic peptides	8.31
23	PGTSGGPA	51.036	642.297	8	37.64	−0.512	non-toxic peptides	5.96
24	PGAEGPAG	50.310	654.297	8	22.21	−0.537	non-toxic peptides	4.00
25	GPKGEPGI	50.127	753.402	8	2.18	−0.912	non-toxic peptides	6.00
26	FGKKGEDP	49.358	876.434	8	2.18	−1.800	non-toxic peptides	6.07
27	GPSVSGEA	48.761	702.318	8	23.40	−0.188	non-toxic peptides	4.00
28	GPREPGAP	47.916	779.393	8	36.86	−1.475	non-toxic peptides	6.00
29	TLRDATNR	47.198	945.499	8	14.04	−1.475	non-toxic peptides	9.26
30	LGNDLEDA	44.721	845.377	8	22.21	−0.625	non-toxic peptides	3.49
31	GDRGPPGA	44.721	725.346	8	2.18	−1.325	non-toxic peptides	5.84
32	DALMQGQE	44.692	890.380	8	23.40	−0.863	non-toxic peptides	3.67
33	PGDGVSVH	44.611	766.361	8	8.75	−0.188	non-toxic peptides	5.08
34	PGSVEGPA	44.531	712.339	8	32.83	−0.287	non-toxic peptides	4.00
35	KDARTSDW	44.447	977.457	8	8.75	−2.000	non-toxic peptides	5.96
36	ASTPNQQR	43.814	900.441	8	23.40	−2.038	non-toxic peptides	9.79
37	VAGAKRGR	42.773	813.493	8	28.27	−0.738	non-toxic peptides	12.01
38	GTPPGYGQ	42.474	775.350	8	0.99	−1.238	non-toxic peptides	5.52
39	SGVRAYFQ	41.502	926.461	8	8.75	−0.212	non-toxic peptides	8.46
40	PGQTEVFQ	41.227	904.429	8	32.83	−0.775	non-toxic peptides	4.00
41	SADCSEKH	40.103	875.344	8	22.21	−1.425	non-toxic peptides	5.30
42	ETEGLKGE	39.663	861.408	8	2.18	−1.512	non-toxic peptides	4.25
43	DVAASREA	39.218	817.393	8	32.83	−0.338	non-toxic peptides	4.37
44	QGPDAGAP	39.218	711.319	8	12.79	−0.925	non-toxic peptides	3.80
45	GPSGPYGP	38.836	730.329	8	22.21	−1.012	non-toxic peptides	5.52
46	MATPLYEY	38.836	986.442	8	14.75	−0.113	non-toxic peptides	4.00
47	TAANGGPA	38.818	657.308	8	29.46	−0.150	non-toxic peptides	5.19
48	GKTGGGLT	38.806	689.371	8	18.38	−0.388	non-toxic peptides	8.75
49	RTRKDSIQ	38.238	1002.557	8	32.83	−2.112	non-toxic peptides	10.84
50	RLAANGLR	36.975	869.520	8	14.04	−0.212	non-toxic peptides	12.00
51	TQLLLHKP	36.557	948.576	8	19.50	−0.188	non-toxic peptides	8.44
52	PGGRLGAP	36.556	723.403	8	37.64	−0.412	non-toxic peptides	10.18
53	STPAQNPR	36.185	869.436	8	19.80	−1.800	non-toxic peptides	9.47
54	AAERAGAP	35.633	741.377	8	22.21	−0.350	non-toxic peptides	6.05
55	KLSSKLSR	35.445	917.566	8	35.68	−0.887	non-toxic peptides	11.17
56	GPKAFYKG	35.105	866.465	8	38.89	−0.863	non-toxic peptides	9.70
57	VGSPHTDF	34.892	858.387	8	34.21	−0.400	non-toxic peptides	5.08
58	QPRGAGPA	34.892	752.393	8	26.25	−1.050	non-toxic peptides	9.75
59	TTGRNPSL	34.824	844.440	8	34.04	−1.050	non-toxic peptides	9.41
60	KDGKNWNS	34.824	947.446	8	0.60	−2.550	non-toxic peptides	8.59
61	GPEGGKGQ	34.717	728.345	8	24.67	−1.762	non-toxic peptides	6.00
62	LGDGGFQR	34.717	848.414	8	24.18	−0.762	non-toxic peptides	5.84
63	PGFQDVHV	34.705	897.434	8	32.83	−0.125	non-toxic peptides	5.08
64	PGGVADRQ	34.705	798.398	8	28.21	−0.988	non-toxic peptides	6.27
65	QVAQDIGR	34.173	885.467	8	23.40	−0.613	non-toxic peptides	5.84
66	KSQAMKGG	34.003	805.412	8	37.64	−1.150	non-toxic peptides	10.00
67	IGNAHGLQ	33.813	808.419	8	15.31	−0.113	non-toxic peptides	6.74
68	AGPGGSKL	33.813	685.376	8	13.56	−0.237	non-toxic peptides	8.80
69	VSGYPTFK	33.813	897.460	8	10.20	−0.212	non-toxic peptides	8.56
70	TTAAPRKP	33.738	840.482	8	13.98	−1.175	non-toxic peptides	11.00
71	AGPYTQER	33.738	920.435	8	12.79	−1.712	non-toxic peptides	6.05
72	VGLPGQRG	33.738	782.440	8	11.60	−0.350	non-toxic peptides	9.72
73	PGSNPKKA	33.738	797.440	8	5.15	−1.738	non-toxic peptides	10.02
74	LKGVAARQ	33.516	841.513	8	11.60	−0.087	non-toxic peptides	11.00

(*continued on next page*)

Table 1 (*continued*)

Number	Sequence	Score	Mass	Length	Instability index	GRAVY	Toxic peptide	Isoelectric point
75	GNEKMKLE	33.396	947.475	8	28.27	−1.625	non-toxic peptides	6.14
76	PGGATGGA	32.971	586.271	8	7.76	−0.037	non-toxic peptides	5.96
77	GPGPLHAQ	32.929	775.398	8	8.75	−0.637	non-toxic peptides	6.74
78	RPSTWGAP	32.470	870.435	8	38.61	−1.087	non-toxic peptides	9.75
79	GPATKTAS	32.470	731.381	8	32.83	−0.562	non-toxic peptides	8.75
80	SGPTPFKL	32.065	845.465	8	3.43	−0.300	non-toxic peptides	8.47
81	PGLTH	31.921	523.275	5	8.00	−0.420	non-toxic peptides	7.17
82	PGSLTIQP	31.303	811.444	8	32.83	−0.037	non-toxic peptides	5.96
83	GPDGGGPK	31.303	683.324	8	30.18	−1.525	non-toxic peptides	5.84
84	YGPGGAAR	31.303	747.366	8	2.95	−0.625	non-toxic peptides	8.75
85	AVQQAQGR	31.289	856.452	8	32.83	−0.950	non-toxic peptides	9.79
86	PGSDKPSW	31.289	872.403	8	12.79	−1.688	non-toxic peptides	6.26
87	STAPRYEN	31.289	936.430	8	4.55	−1.762	non-toxic peptides	5.72
88	YLTFFQKY	31.229	1108.559	8	24.18	−0.163	non-toxic peptides	8.50
89	GPKGEPGH	31.058	777.377	8	12.79	−1.875	non-toxic peptides	6.75
90	ENAFSGGP	31.004	777.329	8	24.18	−0.700	non-toxic peptides	4.00
91	QWHLVYGY	30.718	1064.508	8	7.70	−0.325	non-toxic peptides	6.74
92	GPATSWPL	30.669	827.418	8	32.83	−0.050	non-toxic peptides	5.52
93	EGWGKPAG	30.669	800.382	8	15.25	−1.163	non-toxic peptides	6.10
94	TLNLPQCQ	30.612	915.448	8	38.05	−0.338	non-toxic peptides	5.18
95	DKQNTMGD	30.612	907.371	8	17.12	−2.138	non-toxic peptides	4.21
96	GPQGKSGA	30.612	700.350	8	11.60	−1.150	non-toxic peptides	8.75
97	DEVQKAVA	30.612	858.445	8	8.75	−0.300	non-toxic peptides	4.37
98	SSKGFGVK	30.185	808.444	8	18.61	−0.400	non-toxic peptides	10.00
99	TGKERPGS	30.185	830.425	8	11.60	−1.975	non-toxic peptides	8.41
100	VNTQPDIC	30.185	888.401	8	3.36	−0.200	non-toxic peptides	3.80

peptides with an instability index greater than 40 were considered to be less stable in vitro and thus were not candidates for AFPs (Liang et al., 2025). Finally, 100 AFPs that met the above conditions and had the highest ion scores were screened for molecular docking to investigate the binding pattern of cod collagen peptides with ice crystals.

3.8. Molecular docking

The molecular docking results of 100 AFPs are detailed in Table S4 (Supplementary material). The binding affinities of AFPs to ice crystals, as indicated by their docking energies, ranged from −2.5 to −6 kcal/mol (Fig. 4(a)). A lower docking energy score signifies a stronger binding affinity, and interactions with docking energies between −5 and − 15 kcal/mol are deemed stable (Cao et al., 2024). Consequently, 64 of the AFPs were identified as stable for binding with ice crystals. Reports indicate that the binding of AFPs to ice crystalstals and inhibition of their growth is mainly attributed to the formation of hydrogen bonds, hydrophobic interactions, and non-bonding interactions (Jiang et al., 2022). Subsequently, the structures of AFPs, which exhibit the capacity to bind stably with ice crystals, along with the docking results, were comprehensively subjected to statistical analysis. Hydrogen bonding plays a crucial role as the primary force in the interaction between AFPs and ice crystals, as evidenced by studies on the structure and function of AFPs (Majura et al., 2024). The statistical analyses therefore focused on amino acids that were able to form three or more hydrogen bonds with ice crystals.

3.8.1. Analysis of AFP amino acids

Fig. 4(b) shows the amino acids located at different positions in the AFP of CCP-1 that could form three or more hydrogen bonds stably during interaction with ice crystals. Among them, glycine, proline, and alanine were associated with the antifreeze activity of AFP (Cao, Majura, et al., 2023; Chen et al., 2019). Glycine stably facilitates hydrogen bonding when AFPs bind to ice crystals, predominantly occupying positions 1, 5, 6, and 7 of the AFPs (see Fig. 5(a)). This might be This is attributed to the fact that glycine, which constitutes nearly one-third of the total amino acid residues in collagen, is a key component of collagen peptides (Cao, Majura, et al., 2023). However, proline was found at positions 1, 6, and 8 of AFP, while alanine was located at positions 3, 7, and 8. Notably, the capacity of these two amino acids to form hydrogen bonds increased significantly when positioned at the tail of AFP (Fig. 5 (b) and 5(d)). In addition, it has been reported that proline and alanine contain alkyl side chains, which provide a non-polar environment and can form hydrogen bonds with water molecules to inhibit ice crystal growth (Zhang et al., 2024). This indicates that proline and alanine could not only contribute to the inhibition of ice crystal growth by AFP but also provide a non-polar environment to maintain the structural stability of the peptide itself.

Notably, Table S5 (Supplementary Material) statistics revealed that glutamate and glutamine were more capable of forming hydrogen bonds with water molecules when located at the end of the polypeptide. This was due to the fact that glutamic acid and glutamine have strong polar hydroxyl groups associated with ice affinity (Cao, Cai, et al., 2023), and when located at the end of the peptide, their C-terminal (carboxyl-terminal) end was no longer dehydrated and condensed with other amino acids to form a peptide bond; the carboxyl group was retained, allowing for the formation of more hydrogen bonds with water molecules (Fig. 5 (c) and 5(e)). Furthermore, it was observed in Fig. 4(c) that there was a positive correlation between the three amino acids (glycine, proline, and alanine) associated with the antifreeze activity of AFP, suggesting a synergistic effect between hydrophilic and hydrophobic amino acids during the interaction of AFP with ice crystals. In addition, the positive correlations between cysteine and histidine, as well as between tryptophan and aspartic acid, indicated that AFPs also exhibited synergistic effects between hydrophilic amino acids and acidic or alkaline amino acids during their interaction with ice crystals.

3.8.2. Structural stability analysis of AFPs

Fig. 4(d) shows the forces involved in the formation of amino acid residues within AFP. Arginine, glutamine, and glycine residues could form hydrogen bonds among themselves or with other identical amino acids in the peptide, stabilizing its structure. The oxygen atom in the C-terminal (-C=O) of glycine could form a hydrogen bond with the hydrogen atom of its R group, and the hydrogen atom in the N-terminal ($-NH_2$) could form hydrogen bonds with the C-terminal oxygen atom of another glycine within the peptide structure. However, the hydrogen atom in the guanidine group (=NH) of the R group of arginine formed a hydrogen bond with the oxygen atom in the C-terminus (-C=O). In addition, the hydrogen atom at the N-terminus ($-NH_2$) of glutamine was able to form hydrogen bonds with the oxygen atom in its R group (-C=O)

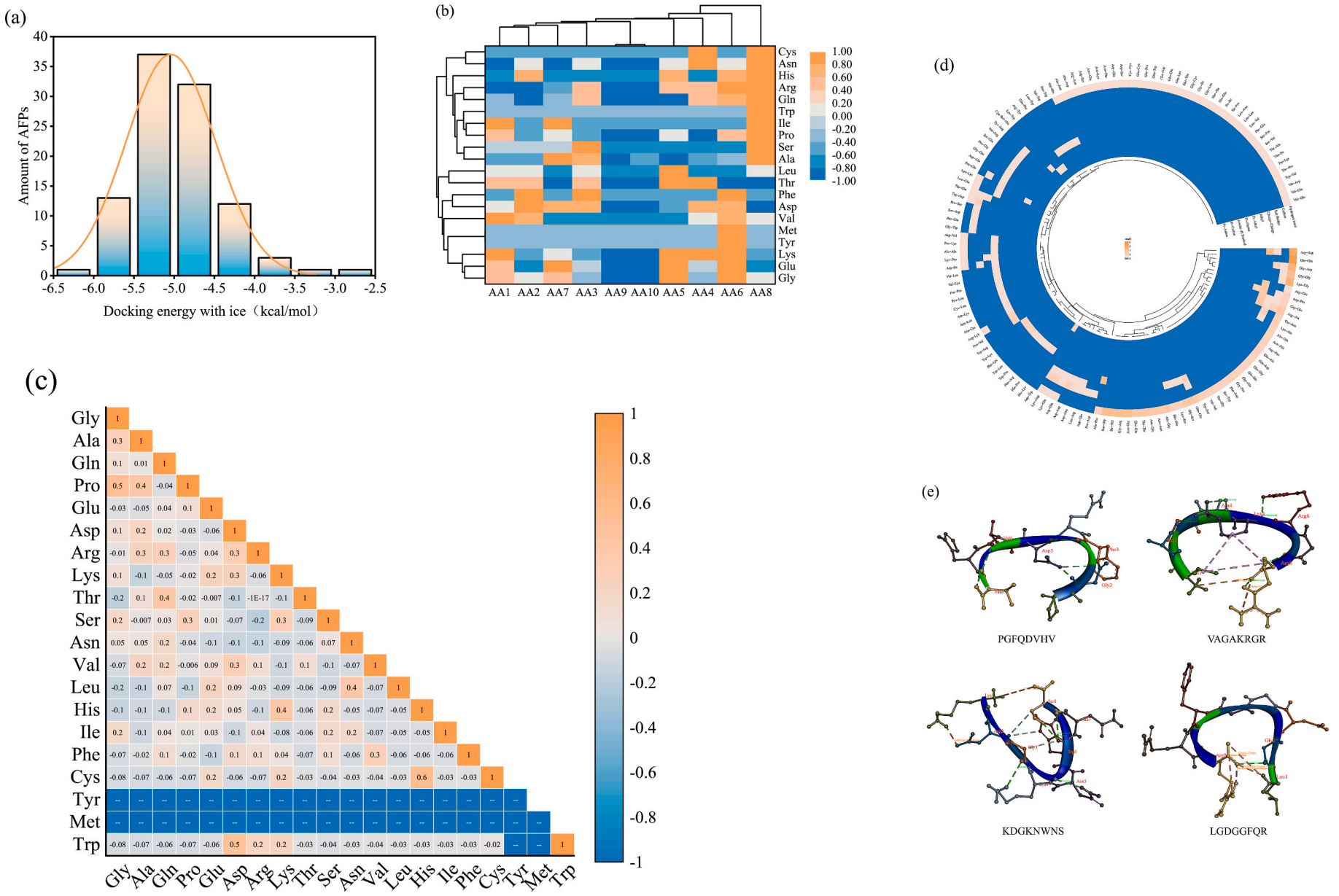

Fig. 4. Distribution map of molecular docking energies for 100 antifreeze peptides (a). Clustering heatmap of the structural relationship between amino acids and antifreeze peptides (b). Correlation heatmap of amino acids in antifreeze peptides (c). Circular clustering heatmap of the interactions between amino acids in antifreeze peptides (d). Schematic diagram of the characteristics of forces that maintain the structural stability of antifreeze peptides (e).

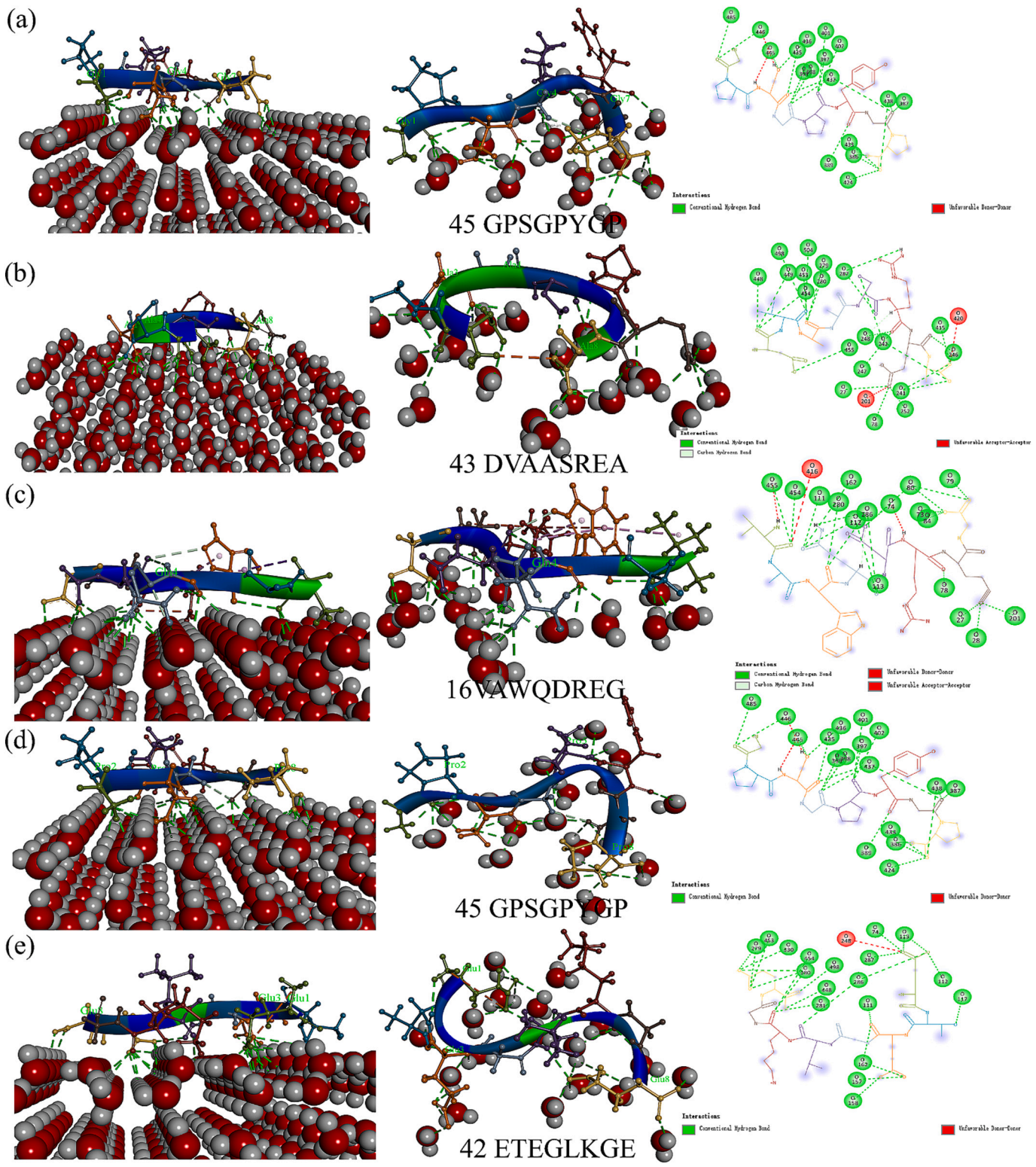

Fig. 5. Molecular docking results of glycine (a), alanine (b), glutamine (c), proline (d) and glutamic (e) acid interactions with ice crystals in antifreeze peptides.

and even with the oxygen atom on the C-terminus (-C=O) of another amino acid. It was reported that the strongest hydrogen bonds were mainly NH-O and OH-O interactions (Edwards & Hamley, 2017). Therefore, the robust capacity of arginine and glutamine to establish hydrogen bonds with water molecules primarily stems from the hydrogen atoms on their amino groups interacting with oxygen atoms.

Highlighting the influence of interactions between alkyl-group-bearing hydrophobic amino acids and the side chains of other hydrophobic residues on peptide structural stability is crucial. Fig. 4(e) demonstrates the formation of a triangular alkyl group among valine, arginine, and lysine residues, while alkyl chains typically induce hydrophobic interactions (Edwards & Hamley, 2017). Consequently, certain AFPs enhance the hydrophobic interactions within the peptide structure. Through the formation of alkyl chains, thus maintaining the

structural stability of AFPs when interacting with ice crystals. In addition, salt bridges and electrostatic interactions were mainly forces formed by -NH_3^+ of alkaline or acidic amino acids with -COO^-. Salt bridges contribute to the structural rigidity of AFPs, as evidenced by their ability to stabilize protein structures and affect protein function, while concurrently reducing the flexibility of these structures (Basu & Biswas, 2018). This indicated that charged amino acids made an important contribution to the formation of hydrogen bonds during the binding of AFP to ice crystals and to the formation of forces that stabilize the structure of the peptide.

3.9. The rules of AFP binding with ice crystals in CCP-1

As shown in Fig. 6, the interaction process between the AFPs in CCP-1 and ice crystals primarily involved two aspects. During this process, hydrophilic and hydrophobic amino acids collaborated to maximize the formation of hydrogen bonds with water molecules, simultaneously aiding in maintaining the structural integrity of AFPs. In terms of forming hydrogen bonds with water molecules, the most numerous conventional hydrogen bonds were formed by the interaction between the oxygen atoms in amino acid residues and the hydrogen atoms in water molecules. Moreover, the (C=O) and (-OH) groups present on amino acid residues have the capability to interact with water molecules, leading to the formation of extra hydrogen bonds. For example,

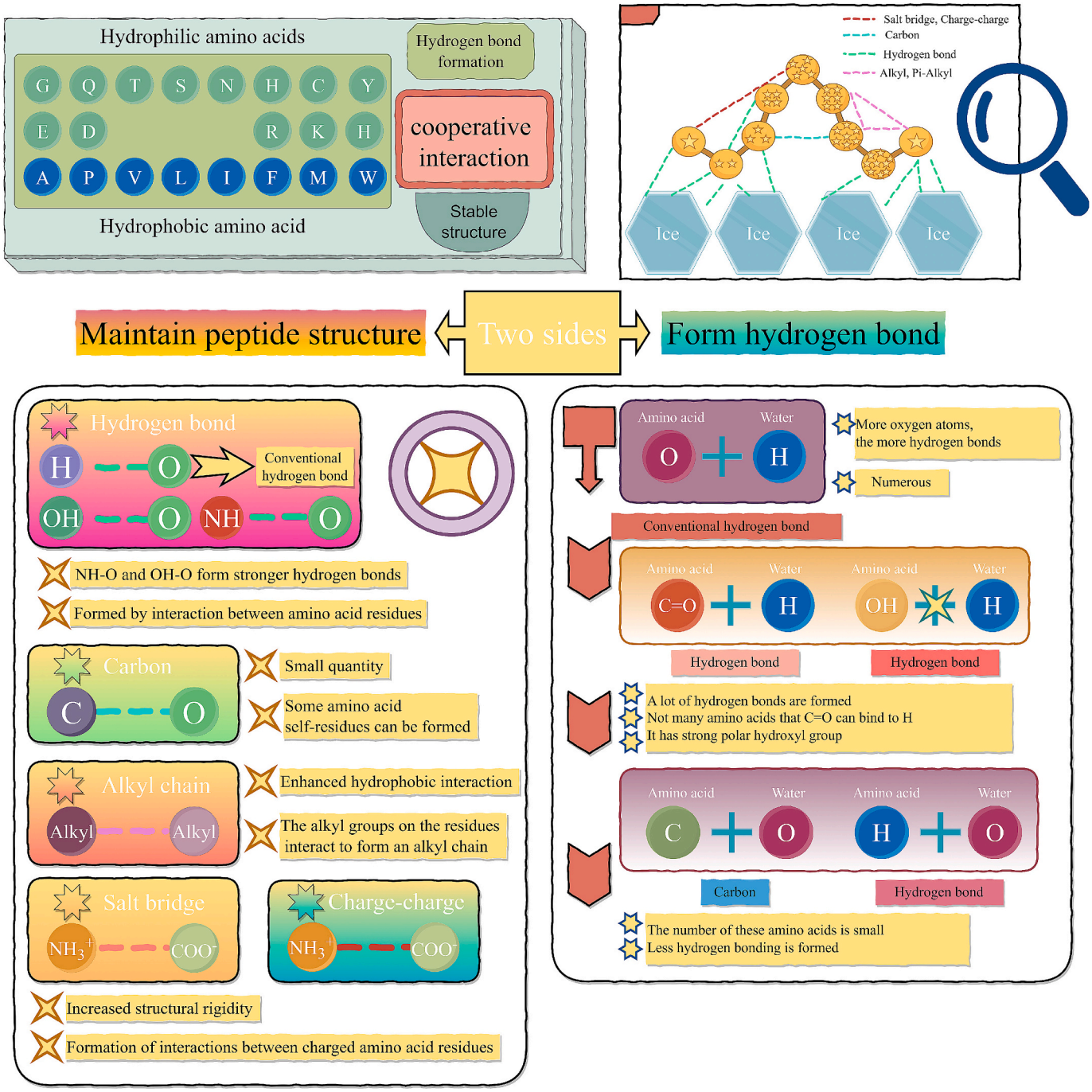

Fig. 6. Mechanism of CCP-1 antifreeze peptide interaction with ice crystals map.

glutamic acid has a strong polar hydroxyl group (-OH) that can form hydrogen bonds, which is associated with its affinity to ice (Cao, Cai, et al., 2023). In addition, the carbon or hydrogen atoms of amino acid residues interacted with the oxygen atoms in water molecules to form hydrogen bonds. Although this type of bonding was less common, its contribution to the interaction process with ice crystals could not be overlooked. The stability of peptide structures is primarily maintained through hydrogen bonds, salt bridges, electrostatic interactions, and hydrophobic effects, with alkyl side chains playing a significant role. Among these, in addition to conventional hydrogen bonds, the hydrogen bonds formed by NH-O and OH-O interactions played a crucial role in maintaining the stability of peptide structures, being the strongest components. Simultaneously, the salt bridges and electrostatic interactions between charged amino acid residues ($-NH_3^+$ and $-COO^-$) cannot be overlooked, as they contribute to the AFP structure's stability by imparting local rigidity. Furthermore, amino acids with alkyl groups interacted to form alkyl side chains, enhancing the hydrophobic properties of the structure. Interactions within the peptide structure, which was beneficial for the stability of the AFP structure.

In summary, the ability of AFPs to interact with ice crystals is closely related to their primary structure, as evidenced by the combined role of hydrophilic and hydrophobic amino acids in this process. Hydrophilic amino acids (glycine, alkaline amino acids, and, acidic amino acids) can form hydrogen bonds with water molecules. It also interacts with itself or other amino acids via characteristic functional groups present in the amino acid residues, thereby maintaining the stability of the peptide structure. Through intermolecular forces (hydrogen bonding, alkyl side chains, salt bridges, and electrostatic interactions). Hydrophobic amino acids (proline, alanine) can interact with water molecules to form hydrogen bonds while providing a local hydrophobic environment. Notably, the ability of amino acids to form hydrogen bonds with water molecules was limited by their position in the primary structure of the AFP. When these amino acids (residues containing -OH as well as -NH) are located at the end of AFP, the interaction of the AFP with ice crystals is facilitated to a greater extent.

4. Conclusions

In this study, the cryoprotective effect of CCP-1 on repeated F-T surimi and its binding pattern with ice crystals were investigated at the molecular level. The results indicated that CCP-1 effectively hindered MP unfolding during F-T cycles and minimized tryptophan exposure within MP, consequently slowing down the decline in Ca^{2+}-ATPase activity. The antifreeze effect of the CCP-1 (1 %, 3 % (*w*/w)) treatment group was better than that of commercial antifreeze compound phosphate (0.5 % (*w*/w)) and was positively correlated with its concentration. CCP-1 has the potential to be a new phosphorus-free antifreeze that replaces traditional commercial antifreeze and reduces the addition of polyphosphates to surimi. Further, molecular docking statistics showed that the ability of AFP in CCP-1 to interact with ice crystals was closely linked to its primary structure and that hydrophilic and hydrophobic amino acids worked together in this process. More importantly, alkaline and acidic amino acids maintain the stability of the peptide structure through electrostatic interaction forces. The residues contain $-NH_3^+$ and $-COO^-$, which could form stronger hydrogen bonds with water molecules so that the AFP could bind more stably with ice crystals. It played an important role in the interaction process with ice crystals. Further, the ability of amino acids to form hydrogen bonds is limited by their position in the primary structure of AFP. When amino acids (residues containing -OH and -NH) are at the terminal of AFP, they were able to form more hydrogen bonds, allowing the interaction of AFP with ice crystals to be facilitated to a greater extent. These findings validate the antifreeze activity of CCP-1 and its binding pattern with ice crystals in the future, the relationship between the amino acids sequence in the primary structure of AFP, and its antifreeze activity to fully understand the underlying intricacies.

CRediT authorship contribution statement

Jiajian Liang: Writing – original draft, Methodology, Investigation, Data curation. **Xiujuan Chen:** Data curation. **Mingtang Tan:** Writing – review & editing. **Zhongqin Chen:** Software, Methodology, Investigation. **Haisheng Lin:** Software, Methodology. **Jialong Gao:** Writing – review & editing. **Huina Zheng:** Writing – review & editing. **Wenhong Cao:** Validation, Supervision, Funding acquisition, Conceptualization.

Declaration of competing interest

The authors declare that they have no known competing financial interests or personal relationships that could have appeared to influence the work reported in this paper.

Acknowledgments

This work was supported by the Shenzhen Science and Technology Program (JCYJ20220530162011026). We gratefully acknowledge the anonymous referees for the comments and constructive suggestions provided for improving the manuscript.

Appendix A. Supplementary data

Supplementary data to this article can be found online at https://doi.org/10.1016/j.fochx.2025.102334.

Data availability

Data will be made available on request.

References

Basu, S., & Biswas, P. (2018). Salt-bridge dynamics in intrinsically disordered proteins: A trade-off between electrostatic interactions and structural flexibility. *Biochimica et Biophysica Acta (BBA) - Proteins and Proteomics, 1866*(5–6), 624–641. https://doi.org/10.1016/j.bbapap.2018.03.002

Cao, C. C., Kang, H., Mu, Y. H., Zhang, J. N., Sun, W. Z., Zhao, M. M., & Su, G. W. (2024). Isolation and identification of novel umami-enhancing peptides from fermented soybean meal hydrolysate by consecutive chromatography and UPLC–ESI–QTOF–MS/MS. *food. Bioscience, 58*, Article 103661. https://doi.org/10.1016/j.fbio.2024.103661

Cao, L., Majura, J. J., Liu, L., Cao, W. H., Chen, Z. Q., Zhu, G. P., … Lin, H. S. (2023). The cryoprotective activity of tilapia skin collagen hydrolysate and the structure elucidation of its antifreeze peptide. *LWT, 179*, Article 114670. https://doi.org/10.1016/j.lwt.2023.114670

Cao, S. Q., Cai, J. X., Wang, X. Z., Zhou, K. N., Liu, L., He, L. Y., … Yang, H. (2023). Cryoprotective effect of collagen hydrolysates from squid skin on frozen shrimp and characterizations of its antifreeze peptides. *LWT, 174*, Article 114443. https://doi.org/10.1016/j.lwt.2023.114443

Chen, X., Li, X. Z., Yang, F. J., Wu, J. H., Huang, D., Huang, J. L., & Wang, S. Y. (2022). Effects and mechanism of antifreeze peptides from silver carp scales on the freeze-thaw stability of frozen surimi. *Food Chemistry, 396*, Article 133717. https://doi.org/10.1016/j.foodchem.2022.133717

Chen, X., Shi, X. D., Cai, X. X., Yang, F. J., Li, L., Wu, J. H., & Wang, S. Y. (2020). Ice-binding proteins: A remarkable ice crystal regulator for frozen foods. *Critical Reviews in Food Science and Nutrition, 61*(20), 3436–3449. https://doi.org/10.1080/10408398.2020.1798354

Chen, X., Wu, J. H., Li, X. Z., Yang, F. J., Yu, L. H., Li, X. K., … Wang, S. Y. (2022). Investigation of the cryoprotective mechanism and effect on quality characteristics of surimi during freezing storage by antifreeze peptides. *Food Chemistry, 371*, Article 131054. https://doi.org/10.1016/j.foodchem.2021.131054

Chen, X., Wu, J. H., & Wang, S. Y. (2019). Cryoprotective activity and action mechanism of antifreeze peptides obtained from tilapia scales on *Streptococcus thermophilus* during cold stress. *Journal of Agricultural and Food Chemistry, 67*(7), 1918–1926. https://doi.org/10.1021/acs.jafc.8b06514

Cheung, I. W. Y., Liceaga, A. M., & Li-Chan, E. C. Y. (2009). Pacific hake (*Merluccius productus*) hydrolysates as Cryoprotective agents in frozen Pacific cod fillet mince. *Journal of Food Science, 74*(8), C588–C594. https://doi.org/10.1111/j.1750-3841.2009.01307.x

Coppola, D., Oliviero, M., Vitale, G. A., Lauritano, C., D'Ambra, I., Iannace, S., & Pascale, D. D. (2020). Marine collagen from alternative and sustainable sources: Extraction, processing and applications. *Marine Drugs, 18*(4), 214. https://doi.org/10.3390/md18040214

Edwards, G. C. J. C., & Hamley, I. W. (2017). Self-assembly of bioactive peptides, peptide conjugates, and peptide mimetic materials. *Organic & Biomolecular Chemistry, 15*, 5867–5876. https://doi.org/10.1039/c7ob01092c

Fu, W. Q., Wang, P. X., Chen, Y. Y., Lin, J. X., Zheng, B. D., & Zhang, Y. (2019). Preparation, primary structure and antifreeze activity of antifreeze peptides from *Scomberomorus niphonius* skin. *LWT, 101*, 670–677. https://doi.org/10.1016/j.lwt.2018.11.067

Hu, Y. P., Gao, Y. F., Solangi, I., Liu, S. C., & Zhu, J. (2022). Effects of tea polyphenols on the conformational, functional, and morphological characteristics of beef myofibrillar proteins. *LWT, 154*, Article 112596. https://doi.org/10.1016/j.lwt.2021.112596

Jiang, W. T., Yang, F. J., Chen, X., Cai, X. X., Wu, J. H., Du, M., … Wang, S. Y. (2022). Molecular simulation -based research on antifreeze peptides: Advances and perspectives. *Journal of Future Foods, 2*(3), 203–212. https://doi.org/10.1016/j.jfutfo.2022.06.002

Karnjanapratum, S., & Benjakul, S. (2015). Cryoprotective and antioxidative effects of gelatin hydrolysate from unicorn leatherjacket skin. *International Journal of Refrigeration, 49*, 69–78. https://doi.org/10.1016/j.ijrefrig.2014.09.016

Li, F. F., Wang, B., Kong, B. H., Shi, S., & Xia, X. F. (2019). Decreased gelling properties of protein in mirror carp (*Cyprinus carpio*) are due to protein aggregation and structure deterioration when subjected to freeze-thaw cycles. *Food Hydrocolloids, 97*, Article 105223. https://doi.org/10.1016/j.foodhyd.2019.105223

Li, F. F., Wang, B., Liu, Q., Chen, Q., Zhang, H. W., Xia, X. F., & Kong, B. H. (2018). Changes in myofibrillar protein gel quality of porcine *longissimus* muscle induced by its structural modification under different thawing methods. *Meat Science, 147*, 108–115. https://doi.org/10.1016/j.meatsci.2018.09.003

Li, J. G., Sun, C. H., Yue, X. N., Ma, W. C., Wang, Y., Zhao, J. S., … Bai, Y. H. (2025). Ultrasound-assisted immersion freezing improves the digestion properties of beef myofibrillar protein. *Food Chemistry: X, 25*, Article 102144. https://doi.org/10.1016/j.fochx.2024.102144

Li, M. M., He, S. F., Sun, Y. Y., Pan, D. D., Zhou, C. Y., & He, J. (2023). Effectiveness of L-arginine/L-lysine in retarding deterioration of structural and gelling properties of duck meat myofibrillar protein during freeze-thaw cycles. *Food Bioscience, 51*, Article 102302. https://doi.org/10.1016/j.fbio.2022.102302

Li, Z. Y., Wang, Q., Li, S. T., Chang, Y., Zheng, X., Cao, H., & Zheng, Y. F. (2022). Usage of nanocrystalline cellulose as a novel cryoprotective substance for the *Nemipterus virgatus* surimi during frozen storage. *Food Chemistry: X, 16*, Article 100506. https://doi.org/10.1016/j.fochx.2022.100506

Liang, J. J., Chen, X. J., Majura, J. J., Tan, M. T., Chen, Z. Q., Gao, J. L., & Cao, W. H. (2025). Insight into the structure-activity relationship of thermal hysteresis activity of cod collagen peptides through peptidomics and bioinformatics approaches. *Food Chemistry, 463*, Article 141514. https://doi.org/10.1016/j.foodchem.2024.141514

Liu, Z. L., Yang, W. G., Wei, H. M., Deng, S. G., Yu, X. X., & Huang, T. (2023). The mechanisms and applications of cryoprotectants in aquatic products: An overview. *Food Chemistry, 408*, Article 135202. https://doi.org/10.1016/j.foodchem.2022.135202

Majura, J. J., Chen, X. J., Chen, Z. Q., Tan, M. T., Zhu, G. P., Gao, J. L., … Cao, W. H. (2024). The cryoprotective effect of *Litopenaeus vannamei* head-derived peptides and its ice-binding mechanism. *Current Research in Food Science, 9*, Article 100886. https://doi.org/10.1016/j.crfs.2024.100886

Mi, H. B., Zhang, Y. H., Zhao, Y. M., Li, J. R., Chen, J. X., & Li, X. P. (2024). Cryoprotective effect of soluble soybean polysaccharides and enzymatic hydrolysates on the myofibrillar protein of *Nemipterus virgatus* surimi. *Food Chemistry, 446*, Article 138903. https://doi.org/10.1016/j.foodchem.2024.138903

Ouyang, J., Han, M., Majura, J. J., Chen, X. J., Tan, M. T., Chen, Z. Q., … Cao, W. H. (2024). Improvement of the antifreeze activity of tilapia skin collagen peptides through enzymatic supramolecular assembly approach. *International Journal of Food Science & Technology, 59*(5), 3360–3372. https://doi.org/10.1111/ijfs.17082

Pan, N., Hu, Y. F., Li, Y., Ren, Y. M., Kong, B. H., & Xia, X. F. (2021). Changes in the thermal stability and structure of myofibrillar protein from quick-frozen pork patties with different fat addition under freeze-thaw cycles. *Meat Science, 175*, Article 108420. https://doi.org/10.1016/j.meatsci.2020.108420

Pinilla, C. M. B., Brandelli, A., López-Caballero, M. E., Montero, P., & Gómez-Guillén, M. D. C. (2022). Structural features of myofibrillar fish protein interacting with phosphatidylcholine liposomes. *Food Research International, 137*, Article 109687. https://doi.org/10.1016/j.foodres.2020.109687

Shi, H. B., Zhang, M. X., Liu, X. C., Yao, X. Q., Wang, W., Zheng, J. B., … Sun, W. Z. (2024). Improved qualities of salt-reduced tilapia surimi by adding konjac glucomannan: Insight into the edible traits, gel properties and anti-freezing ability. *Food Hydrocolloids, 153*, Article 109971. https://doi.org/10.1016/j.foodhyd.2024.109971

Stevens, J. R., Newton, R. W., Tlusty, M., & Little, D. C. (2018). The rise of aquaculture by-products: Increasing food production, value, and sustainability through strategic utilization. *Marine Policy, 90*, 115–124. https://doi.org/10.1016/j.marpol.2017.12.027

Tan, G. Z., Yue, N., Sun, C. N., Bu, Y., Zhang, X. M., Zhu, W. H., … Li, X. P. (2024). Effects of plasma-activated slightly acidic electrolyzed water on salmon myofibrillar protein: Insights from structure and molecular docking. *Food Chemistry: X, 22*, Article 101389. https://doi.org/10.1016/j.fochx.2024.101389

Vidal, L. A., Aguilar, T. J. E., & Liceaga, A. M. (2022). Integration of molecular docking analysis and molecular dynamics simulations for studying food proteins and bioactive peptides. *Journal of Agricultural and Food Chemistry, 70*(4), 934–943. https://doi.org/10.1021/acs.jafc.1c06110

Wang, W. X., Bu, Y., Li, W. Z., Zhu, W. H., Li, J. R., & Li, X. P. (2024). Effects of nano freezing-thawing on myofibrillar protein of Atlantic salmon fillets: Protein structure and label-free proteomics. *Food Chemistry, 442*, Article 138369. https://doi.org/10.1016/j.foodchem.2024.138369

Yang, F. J., Chen, X., Huang, M. C., Yang, Q., Cai, X. X., Chen, X., … Wang, S. Y. (2021). Molecular characteristics and structure–activity relationships of food-derived bioactive peptides. *Journal of Integrative Agriculture, 20*(9), 2313–2332. https://doi.org/10.1016/S2095-3119(20)63463-3

Yang, F. J., Jiang, W. T., Chen, X., Chen, X., Wu, J. H., Huang, J. L., … Wang, S. Y. (2022). Identification of novel antifreeze peptides from *Takifugu obscurus* skin and molecular mechanism in inhibiting ice crystal growth. *Journal of Agricultural and Food Chemistry, 70*(44), 14148–14156. https://doi.org/10.1021/acs.jafc.2c04393

Yang, F. J., Jiang, W. T., Chen, X., Wu, J. H., Huang, J. H., Cai, X. X., & Wang, S. Y. (2023). Investigation on the quality regulating mechanism of antifreeze peptides on frozen surimi: From macro to micro. *Food Research International, 163*, Article 112299. https://doi.org/10.1016/j.foodres.2022.112299

Zarubin, N. Y., Kharenko, E. N., Bredikhina, O. V., Lavrukhina, E. V., Rysakova, K. S., Novikov, V. Y., … Mikhailova, M. V. (2024). An isotonic drink containing pacific cod (*Gadus macrocephalus*) processing waste collagen hydrolysate for bone and cartilage health. *Marine Drugs, 22*(5), 202. https://doi.org/10.3390/md22050202

Zhang, C. C., Wang, Y. R., Yang, Q., & Chen, H. Q. (2024). Effect of bovine hide gelatin antifreeze peptides on the quality of frozen dough treated with freeze-thaw cycles and its steamed bread. *Journal of Cereal Science, 117*, Article 103924. https://doi.org/10.1016/j.jcs.2024.103924

Zhang, M. C., Li, F. F., Diao, X. P., Kong, B. H., & Xia, X. F. (2017). Moisture migration, microstructure damage and protein structure changes in porcine longissimus muscle as influenced by multiple freeze-thaw cycles. *Meat Science, 133*, 10–18. https://doi.org/10.1016/j.meatsci.2017.05.019

Zhang, Y. M., Dong, M., Zhang, X. Y., Hu, Y. J., Han, M. Y., Xu, X. L., & Zhou, G. H. (2020). Effects of inulin on the gel properties and molecular structure of porcine myosin: A underlying mechanisms study. *Food Hydrocolloids, 108*, Article 105974. https://doi.org/10.1016/j.foodhyd.2020.105974

Zhu, K., Zheng, Z., & Dai, Z. (2022). Identification of antifreeze peptides in shrimp byproducts autolysate using peptidomics and bioinformatics. *Food Chemistry, 383*, Article 132568. https://doi.org/10.1016/j.foodchem.2022.132568

Zhu, S. C., Jin, Y., Yu, J. H., Yang, W. T., Lian, J., Wei, Z. P., … Zhou, X. X. (2024). Composition-antifreeze property relationships of gelatin and the corresponding mechanisms. *International Journal of Biological Macromolecules, 268*(2), Article 131941. https://doi.org/10.1016/j.ijbiomac.2024.131941